Submersible digital in-line holographic microscope

S. K. Jericho, J. Garcia-Sucerquia, Wenbo Xu, M. H. Jericho, and H. J. Kreuzer

Additional information on Rev. Sci. Instrum.

Submersible digital in-line holographic microscope

S. K. Jericho, J. Garcia-Sucerquia,[a)] Wenbo Xu, M. H. Jericho,[b)] and H. J. Kreuzer
Department of Physics and Atmospheric Science, Dalhousie University, Halifax,
Nova Scotia B3H 3J5, Canada

Few instruments exist that can image microscopic marine organisms in their natural environment so that their locomotion mechanisms, feeding habits, and interactions with surfaces, such as biofouling, can be investigated *in situ*. We describe here the design and performance of a simple submersible digital in-line holographic microscope that can image organisms and their motion with micron resolution and that can be deployed from small vessels. Holograms and reconstructed images of several microscopic aquatic organisms were successfully obtained down to a depth of 20 m. Important microscope characteristics such as the effect of camera pixel size on lateral and depth resolutions as well as the maximum sample volume that can be imaged with a given resolution are discussed in detail. © *2006 American Institute of Physics.* [DOI: 10.1063/1.2193827]

INTRODUCTION

In recent years in-line holography with numerical reconstruction, or digital in-line holographic microscopy (DIHM), has been perfected to the point at which submicron resolution is routinely achieved with light. DIHM has been developed into a new tool in such diverse areas as cell biology, microparticle imaging and tracking, and polymer crystallization. Details of the method and a thorough discussion of its history and potential have been presented in a number of publications together with earlier results in the above-mentioned fields.[1–7] The high depth of field that can be achieved with holographic microscopy makes DIHM of particular interest for *in situ* study of marine organisms. Submersible holographic imaging systems have been developed in the past to measure distributions of marine organisms and to determine their size, swimming behavior, and speed. Early attempts at subsea holographic imaging were made by Heflinger *et al.*[8] and Carder *et al.*[9] More recently an in-line analog holography imaging system that is operated from a remotely controlled vehicle was developed by Malkiel *et al.*[10,11] A similar system with in-line as well as off-line capability was also developed by Watson *et al.*[12] These systems are capable of large volume imaging. The large volume that is sampled by these instruments, however, means that high power *Q*-switched lasers have to be employed that can provide pulses in the ns range to obtain sharp images of marine organisms. Holograms are recorded on high-resolution films which allow the imaging of organisms down to 10 μm resolution in liters of water. Use of photographic film puts a severe restriction on the number of holograms that can be recorded in a reasonable time frame and hence puts a restriction on capturing the motion and dynamics of organisms. These systems are necessarily complex and as a result the instruments are heavy and may weigh up to several tons. The first to use digital sensors in an underwater application were Owen and Zozulya[13] who used a charge-coupled device (CCD) array to capture and reconstruct digitally in-line holograms of marine organisms to a depth of 16 ft. Here we report the design and operation of a submersible digital in-line holographic microscope (SDIHM) that uses point source illumination to produce magnified holograms of marine organisms. The instrument is capable of capturing marine organisms and their motion with micron and subsecond resolution. It is extremely simple and compact in design and it can be deployed in a marine environment from small boats. Its simplicity should make it a valuable instrument for the *in situ* study of marine organisms or in the monitoring of marine life through remote sensing. In DIHM image quality and resolution depend sensitively on the physical arrangement of light source, object, and CCD chip as well as on the CCD chip characteristics such as chip width and pixel size. To achieve high-resolution with DIHM over as large a volume as possible, it is important to analyze some of the factors that can lead to image degradation. Such an analysis will also contribute to our understanding of the potential and the limitations of DIHM.

PRINCIPLE OF DIHM

We show a schematic of in-line holography in Fig. 1: A microscope objective focuses light from a laser onto a pinhole, having a diameter of the order of the wavelength, which acts as the "point source" from which a spherical wave of wavelength λ emanates. The wave illuminates an object and forms a geometrically magnified diffraction pattern on a screen, a few centimeters away. In our case the screen is the photosensitive area of a CCD camera. If the amplitudes of scattered waves from the object, shown by the dotted lines in Fig. 1, are small compared with the unscattered reference wave, the interference pattern on the screen constitutes a hologram, linear in the scattered wave. The hologram is stored as a digital image in a computer and it contains the information about all the scattering points lo-

---

[a)]On leave from Physics School Universidad Nacional de Colombia Sede Medellin, A. A. 3840, Medellin-Columbia.
[b)]Electronic mail: jericho@fizz.phys.dal.ca
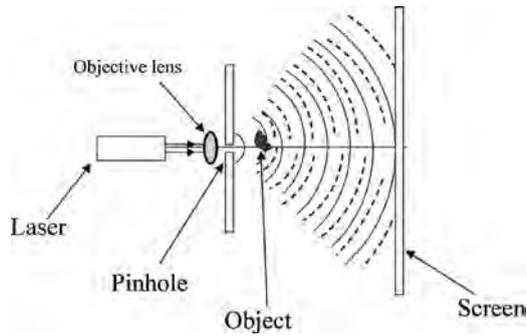
77, 043706-1

FIG. 1. Principle of DIHM. An objective lens focuses a laser on to a pinhole. Spherical waves from the pinhole travel towards a detector screen such as the chip in a CCD camera. At the screen the unscattered reference waves (solid lines) combine with waves scattered by objects (dotted lines) to form a hologram.
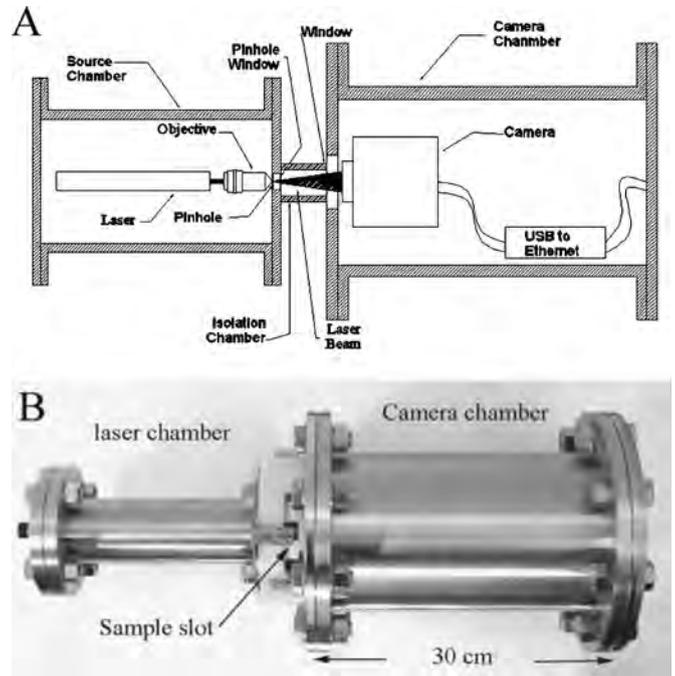

FIG. 2. (A) Schematic diagram of the microscope chambers. The small chamber on the left houses the laser, objective, and pinhole. The larger chamber on the right accommodates the CCD camera, and the USB-2 to ethernet converter. Seawater circulates through the space between the source and camera windows. (B) Photograph of the SDIHM. The sample fluid is circulated through a slot between the laser and camera chambers. The bottom of the slot was closed by a screen (not shown) to exclude larger organisms from the light cone as the instrument is lowered to the desired depth.

cated within the imaging volume. To recover the object wave fronts and hence to obtain the object image, the hologram is reconstructed in this work with the help of a Kirchhoff-Helmoltz transform. The role of reconstruction is to obtain the three-dimensional structure of the scattering points from the two-dimensional hologram on the screen. The Kirchhoff--Helmholtz transform[3],

$$K(\mathbf{r}) = \int_S d^3\xi \tilde{I}(\boldsymbol{\xi}) \exp[2\pi i \boldsymbol{\xi} \cdot \mathbf{r}/\lambda \xi], \tag{1}$$

gives the wave fronts $K(r)$, throughout the imaging volume. The integration extends over the two-dimensional (2D) surface of the screen with coordinates $\xi=(X,Y,D)$, where D is the distance from the source (pinhole) to the center of the screen (CCD chip), and $I(\xi)$ is the contrast image (hologram) on the screen obtained by subtracting the images with and without the object present. The function $K(r)$ is significantly structured and different from zero only in the space region occupied by the object. By reconstructing the wave front $K(r)$ on a number of planes at various distances from the source in the vicinity of the object, a three-dimensional (3D) image can be built up from a single 2D hologram. The plot of $|K(r)|$ on a two-dimensional plane, perpendicular to the optical axis, which we will call a 2D holographic reconstruction, is equivalent to one in-focus image taken in a conventional compound microscope. In DIHM one can generate a stack of 2D holographic reconstructions from a single hologram. Combining such a stack will result in a 3D image of the object; this latter step is usually referred to as 3D reconstruction. The wave front $K(r)$ is a complex function and one usually plots its magnitude to represent the object, although phase images are also available. For the numerical implementation of the transform we have developed a fast algorithm that evaluates $K(r)$ without any approximations. It is incorporated in a self-contained program package, originally applied to electron holography, called LEEPS, that not only performs the numerical reconstruction but also all other procedures connected with data management and visualization.[14]

To obtain high-resolution reconstructions of particle trajectories, we followed the procedure outlined in Ref. 6. The procedure is the following. (i) A sequence of holograms (h_i) is recorded at the maximum frame rate allowed by the camera. (ii) Consecutive hologram pairs are subtracted, pixel by pixel, to generate new holograms i.e., (h_1-h_2), (h_3-h_4), etc. Reconstruction of each difference hologram will show successive positions of any moving objects while the information about stationary objects is subtracted out. The individual reconstructions can then be displayed to show the complete trajectories of the objects. Other subtraction sequences such as (h_1-h_2), (h_1-h_3), etc., are also possible. Successive difference holograms can also be combined into a single data file and the combined file is then reconstructed with the Kirchhoff-Helmholtz transform.[6]

INSTRUMENT

The intrinsic simplicity of DIHM allows for a compact design of a submersible microscope. Figure 2(a) shows a schematic drawing of the two microscope chambers and the optic path. The two chambers are rigidly coupled together with four bolts. The source chamber houses the laser, an objective lens ($100\times$) and pinhole while the recording chamber houses the CCD camera and the data transfer units for the Universal Serial Bus (USB)-2 connection to the computer at the surface. The chambers are standard SS nipples (Kurt Lesker) that are closed with Stainless Steel (SS) flanges that accommodate either the optical windows or the electrical plugs for the electrical connections. The present instrument was designed for lake or coastal waters to a depth of 20 m with flanges that are sealed with viton O rings. The objective lens focuses the laser beam on to the pinhole that is

situated close to a glass window (source window). The nearly spherical waves emanating from the pinhole travel towards the camera chamber and illuminate objects that are located between the source window and the window in front of the CCD camera. The two USB-2 to ether net converters allowed data transmission up to 480 Mbits/s. The optical window on the camera chamber has a diameter of 25 mm and a thickness of 4 mm and is situated about 4 mm from the CCD chip. Construction of the source window is more problematic if high spatial resolution of reconstructed images is desired. As will be explained below, for high resolution, short pinhole to object distances is required. This implies that the source window has to be thin. Since the window is close to the point source, it fortunately also meant that the window could be small in diameter. The source windows therefore had diameters of 2 mm and a thickness of only 150 μm. These windows were pressure tested with argon gas up to 8 atm without rupture.

The lasers used in most of our tests were solid state lasers with wavelengths of 532 or 630 nm and powers between 3 and 15 mW. The laser was mounted coaxially in an aluminum support tube and was held in position by six adjustment screws pointing in a radial direction so that the laser beam could be aligned with the axis of the microscope objective. The 1 μm pinhole was directly mounted on the microscope objective and preadjusted to be coincident with the focus of the objective. The laser-objective-pinhole system was thus built as a single unit point source of light.

The CCD camera was a Lumenera Lu160M with 1392 $\times$1040 pixels, 6.4 μm in size. The camera had a frame rate of 7 f/s and a minimum exposure time of 0.045 ms. This short exposure time ensured that sharp images of microplankton in motion could, in principle, be obtained. The minimum practical exposure time was generally dictated by the light intensity available from the pinhole and was limited to 0.2 ms. In an ocean environment with the SDIHM suspended from a vessel, however, wave action and tidal currents generated excessive motion of the water in the imaging volume and our 0.2 ms exposure time was often inadequate for sharp imaging of organisms. The imaging volume was therefore surrounded by an isolation chamber (not shown) that could be opened to the ocean or closed for imaging with the help of control lines operated from the surface. Figure 2(b) shows a picture of the completed microscope.

For field trials, the holograms were recorded on a laptop computer. The total power consumption including the laptop was 135 W. As power source served a 12 V lead-acid storage battery (100 A h capacity) that fed a voltage converter so that all components could be operated from a 110 V supply.

PERFORMANCE OF THE SUBMERSIBLE MICROSCOPE

Initial instrument testing consisted of imaging a large variety of fresh water organisms obtained from water samples from local ponds and lakes. These were bench tests performed in order to explore the optimum arrangement for imaging organisms with micron resolution. The velocity of aquatic organisms, of 100 μm or less in size, was generally a few hundred μm/s to a few mm/s. To obtain sharp images of
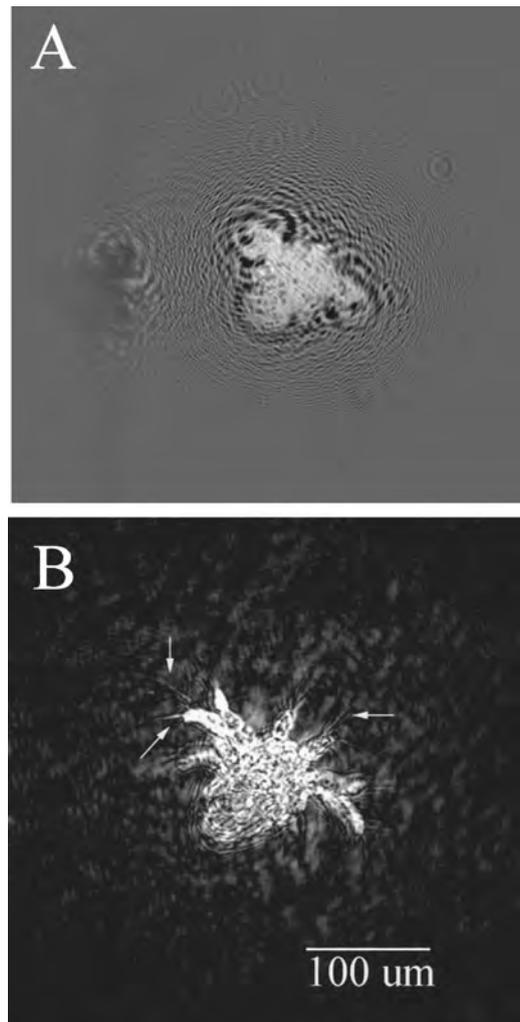

FIG. 3. (A) Hologram of a water mite. (B) Reconstructed image from the hologram in (A). The hairlike protrusions (arrows) from the arms of the mite are $\sim$2–3 μm in diameter. Sample-object distance=1.5 mm; sample-screen distance=13.7 mm; green laser (532 nm) and λ_{eff}=430 nm; exposure time =2 ms. Pinhole size=1 μm.

these, the exposure times were around 0.2 μs. Examples of organisms and their trajectories are shown in the following figures. Figure 3(a) shows a hologram of a water mite obtained from a bench test. The hologram is a contrast hologram which is obtained when the intensity pattern with the object absent is subtracted from the corresponding intensity pattern (hologram) with the object present.[5] The image reconstructed from this hologram is shown in Fig. 3(b). The $\sim$2 μm diameter hairlike protrusions from the arms of the mite, indicated by the arrows in Fig. 3(b), are clearly visible. Figure 4(a) shows a benchtop image of a fresh water rotifer *Philodina* with $\sim$2 μm resolution. Sequences of holograms of these organisms also gave information about their swimming characteristics.

The compact size of our SDIHM made it possible to deploy the instrument in coastal waters from small vessels. A series of tests were performed in Nova Scotia coastal waters to a depth of 18 m (the maximum depth was limited by the length of data transfer and power cables available at the times of the experiments). Figure 4(b) shows an image of a marine ciliate Strombidium conicum. These organisms are

FIG. 5. Two images of the marine ciliate *favella*. The organism was swimming with a velocity of 2.1 mm/s from right to left. Comparison of the two successive images of the organism clearly reveals, as a result of the swimming motion, the movement of the celia at its blunt end. Image taken at a depth of 10 m. Source-screen distance=13.7 mm; source-object distance =3.2 mm; green laser and λ_{eff}=430 nm; exposure time=0.2 ms. The protocol used to image trajectories of organisms is discussed in Ref. 6. Pinhole size=1 μm.

abundant in costal waters of the Atlantic and were imaged frequently. Figure 4(c) shows two successive images of a marine flagellate (unidentified). The time interval between holograms was 143 ms and the organism, propelled by a single flagellum, moved with a speed of 432 μm/s. In its first position on the left, the flagellum is active and visible but out of focus, while it reconstructed well in its second position (white arrow) showing the sharply tapered end (~1 μm width). This illustrates how SDIHM can give detailed information about zoo plankton propulsion while organisms move in their natural environment. This is further illustrated in Fig. 5 where we show two successive images of the marine ciliate *favella*. The ciliate was imaged at a depth of 10 m and it moved with a velocity of 2.1 mm/s. Distribution of internal biomass and the shape of the celia at its blunt end are clearly imaged. With CCD cameras capable of higher frame rates, a detailed recording of cilia movement should be possible.

In spite of the small imaging volume discussed below, it was not difficult to record and reconstruct (with ~1.5 μm resolution) holograms of organisms within a few millimeters of the source window. A succession of images could also reveal the motion of cilia and flagella as well as the swimming speed of the organisms. An example of a portion of a trajectory of a marine organism (unidentified) at a depth of 9 m is shown in Fig. 6. The organism is only 10 μm long and the trajectory starts in a plane that is 3.6 mm from the point source and ends in a plane about 2.4 mm from the source. Thirty-five holograms in total were reconstructed for the trajectory and each hologram produced one in-focus image. These images were then superimposed with the help of photoshop software to create the final trajectory. The time interval between successive positions of the organism is 143 ms. Figure 6 shows that the organism moved in a somewhat irregular manner and at times appeared to rotate and even modify its shape. The maximum speed was about 200 μm/s.

Our measurements at present were limited to a depth of about 20 m. It is straightforward with our present design to extend the imaging depth to 100 m or more and thus make imaging of plankton at the depth of the continental shelf possible. The fast algorithms of the Low Energy Electron Point Source (LEEPS) reconstruction software allowed re-
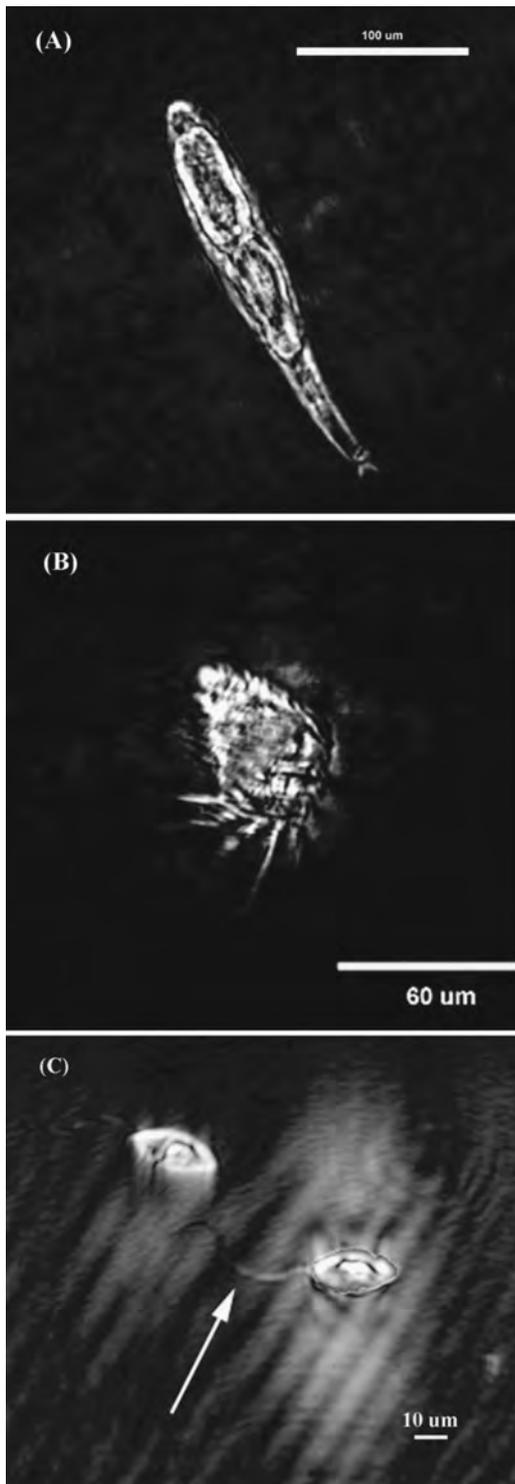

FIG. 4. Reconstructions of a select group of aquatic organisms. (A) Image of the rotifer *Philodina* obtained in a benchtop experiment; exposure time =1 ms. (B) Image of the marine ciliate *Strombidium conicum* imaged from a small vessel in Nova Scotia costal waters. Imaging depth=2 m; source-screen distance=13.7 mm; source-object distance=2 mm; exposure time =0.2 ms. (C) Reconstruction of two successive positions of a marine flagellate. The body has a length of about 28 μm. The single flagellum, about 42 μm in length, is clearly visible in the second image of the organism (arrow). The flagellum has a diameter of about 2 μm near the body of the organism and tapers to less than 1 μm at the end. Exposure time=0.2 ms; depth=10 m; green laser and λ_{eff}=430 nm. Pinhole size=1 μm.
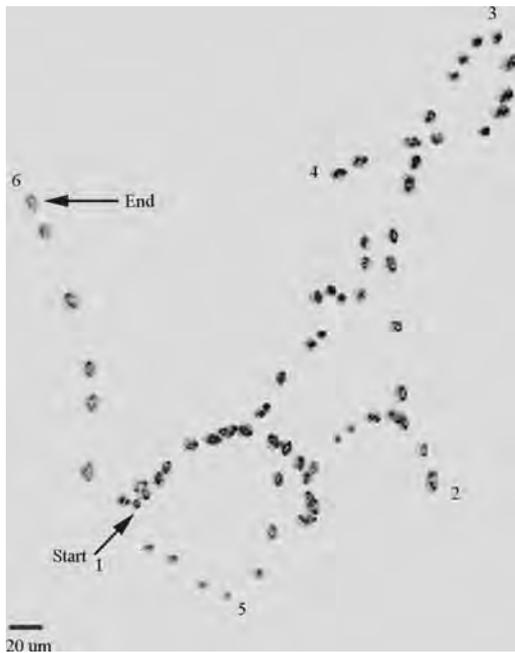
FIG. 6. Projection of the trajectory of a marine organism (not identified but probably a ciliate) imaged at a depth of 9 m. The trajectory is obtained from reconstructions of 50 difference holograms using the subtraction sequence (h_1-h_2), (h_3-h_4), etc., and the sum hologram method as discussed in the text. The depth difference between the start and end position of the trajectory was 1200 μm. The numbers indicate successive sections of the trajectory. The organism appears to tumble and rotate and perhaps also change its shape. Exposure time=0.5 ms; frame rate=7 f/s.

FIG. 7. Schematic arrangement for the discussion of resolution in DIHM. A point source illuminates two point scatterers separated by a distance t and positioned at a source-object distance (D-d). At the CCD chip of half width w, the reference wave and the two scattered waves combine to form the interference pattern calculated with Eq. (2).

construction on a dual core AMD system of a single image plane in 1.0 s (1024×1024 pixels). Reconstructions of 20 image planes (~150 μm between planes) generally gave an adequate representation of the sample volume captured by a single hologram and were obtained in 20 s. To capture the movement of marine organisms, 500 sequential holograms were usually recorded at 7 f/s. A large portion of these (usually 50–250) were then combined into a single hologram as described above. Reconstruction of 100 image planes from such summed holograms gave a depth spacing between planes of 40 μm for our typical sample volume (9 mm³). Detection of most micro organisms in the sampled volume of water could thus be accomplished in 100 s.

RESOLUTION CRITERIA

In the following sections we develop criteria for microscope resolution that allow the determination of microscope parameters for the optimum recording of holograms and thus for optimum resolution. Such an analysis of DIHM is necessary since the information content of a hologram depends sensitively on the relative positioning of source, object, and CCD camera as well as on camera parameters such as pixel size.

As discussed above, DIHM is a two step process consisting of the recording of a hologram followed by the reconstruction of the wave fronts from this hologram in selected planes in the imaged volume. The quality of the reconstructed image clearly depends on the quality of the hologram that contains the information about the imaged objects. Hologram quality depends on a number of factors such as
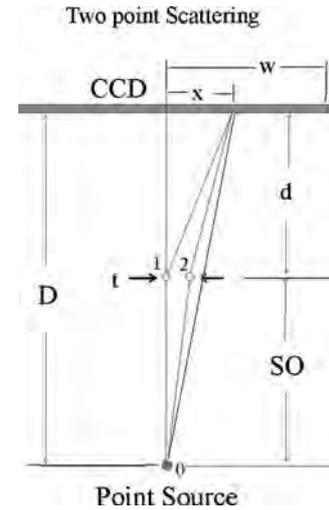
laser wavelength and intensity, pinhole size, size of CCD chip and pixels, distance of point source from CCD chip, object to CCD chip distance (which is related to the numerical aperture), and the quality of the point source of light. Some of these have recently been discussed by Garcia-Sucerquia *et al.*[15] These authors developed criteria for the lateral as well as depth resolution in DIHM. These criteria were tested and confirmed through reconstructions of simulated holograms and through a large range of experimental results in microfluidics and biological applications. Here we aim to determine over what imaging volume a certain resolution is obtainable and what effect CCD camera pixel size has on the resolution.

The volume that can be imaged is defined approximately by the cone that has the CCD chip as the base and the point source as the apex. In the submersible microscope this volume is truncated by the camera chamber window. A discussion of the resolution that can be achieved with DIHM and point source illumination is complicated by the fact that the resolution depends on the position of an object in the imaging volume. The depth of field in DIHM is much larger than that for conventional optical microscopy but resolution depends not only on the object-screen distance (numerical aperture) but also on the source-screen distance and the camera pixel size. This fact makes it difficult at times to find the best physical arrangement of point source, object, and screen for a particular experiment. To address this problem, and to guide the experimentalist in optimizing the resolution in a particular experiment, we examined an idealized experimental setup consisting of a point source, two scattering points, and a CCD screen, as shown in Fig. 7. The point source emits a spherical wave and at the CCD chip this wave interferes with the spherical waves scattered by the two scattering points to form the interference pattern or hologram. The intensity of the scattered waves, I_1 and I_2, at the CCD chip was

assumed to be several orders of magnitude weaker than that from the source, I_0, as required by fundamental holography theory.

For the above arrangement the intensity of the interference pattern on the screen along the x direction can be put into the following simple form:

$$I = I_0 + I_1 + I_2 + 2(I_0 I_1)^{1/2} \cos(\phi_0 - \phi_1)$$
$$+ 2(I_0 I_2)^{1/2} \cos(\phi_0 - \phi_2) + 2(I_1 I_2)^{1/2} \cos(\phi_1 - \phi_2), \tag{2}$$

where the phase factors are $\phi_0 = (2\pi/\lambda)(x^2 + D^2)^{1/2}$, $\phi_1 = (2\pi/\lambda)[(x^2 + d^2)^{1/2} + (D - d)]$, and $\phi_2 = (2\pi/\lambda)\{[(D - d)^2 + t^2]^{1/2} + [d^2 + (x - t)^2]^{1/2}\}$. Here ϕ_0 is the phase factor for the reference wave, and ϕ_1 and ϕ_2 are the phase factors for the on axis (point 1) and off axis (point 2) scattering points in Fig. 7, respectively. I_0, I_1, and I_2 are the intensities at the screen of the reference and the two scattered waves, respectively. Since D and d in Fig. 7 are usually large compared to the width w, the intensities are here treated as constants.

For a single scattering center, such as center 2 in Fig. 7, the 2D interference pattern between the scattered waves from point 2 with the reference wave from point 1 would show the expected concentric rings with ring spacing decreasing as the distance from the center increases. With one scattering center, only the first cosine term in Eq. (2) contributes and Fig. 8(a) shows the one-dimensional (1D) version of the interference pattern along the x direction as calculated from Eq. (2) using parameters consistent with the typical geometry used for our SDIHM. In the evaluation of Eq. (2) we set $I_1 = I_2$ and $I_1/I_0 = 2.7 \times 10^{-4}$. With two scatterers separated by a distance t, both the first and second cosine terms in Eq. (2) contribute to the total intensity, and each scatterer will thus produce a fringe pattern as shown in Fig. 8(a) but each with a slightly different spatial frequency. Since I_1 and I_2 are required to be much less than I_1, the contribution of the last cosine term in Eq. (2) is not significant. The sum of the two individual diffraction patterns produces a fringe modulation whose period depends on the separation distance t between the scattering points. The development of the modulation as t increases is shown in Figs. 8(b) and 8(c). The information about the separation distance t of the scattering points and hence about the resolution is therefore contained in the modulation of the fringe pattern from single scatterers. The resultant fringe pattern thus simply describes a pattern of beats that is generated by the slightly different spacial frequencies $(\phi_0 - \phi_1)/x$ and $(\phi_0 - \phi_2)/x$. Since interference terms such as the third cosine term in Eq. (2) do not contribute, a hologram is therefore a pattern of beats generated from all the scattering points within the imaging cone. It also follows that new holograms can be generated by the simple addition or subtraction of individual holograms provided the dynamic range of the storage medium is not exceeded.

The above arguments lead to a simple relation between resolution and experimental parameters. The minimum requirement for capturing information on the separation of scattering points is to have the first modulation minimum present on the chip (this would be equivalent to the Abbe criterion in conventional optics). If the source-object dis-
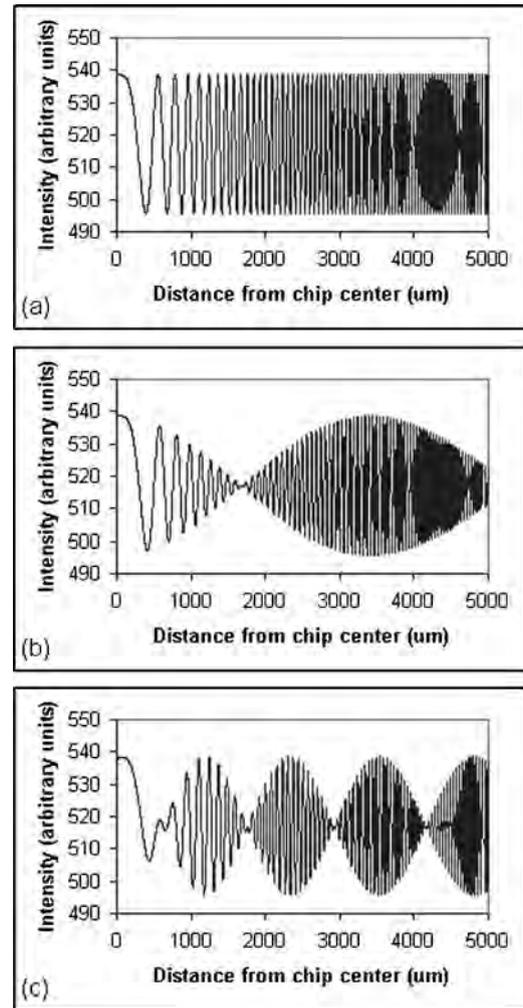

FIG. 8. Example of calculated interference patterns. Calculations are for a source-screen distance of 13.7 mm, an object-screen distance of 13.2 mm, and a wavelength of 422 nm. (a) Interference pattern for a single scattering point. This represents the basic pattern of the interference fringes. (b) Interference pattern for a separation of the scattering points of 1.5 μm. The first modulation maximum is 3500 μm from the chip center. (c) Interference pattern for a separation of the scattering points of 5 μm. At this separation, several modulation maxima are captured.

tance is large compared to the separation t between scattering points (which is so in most cases), then the condition for a modulation minimum is[15]

$$(2\pi/\lambda)(r_1 - r_2) = n\pi. \tag{3}$$

This leads to the following simple relation between t and the position x of the first minimum on a screen:

$$x = (\lambda/2)d/[t^2 - (\lambda/2)^2]^{1/2}$$

or

$$t/\lambda = \left(\tfrac{1}{2}\right)\{(d/x)^2 + 1\}^{1/2}. \tag{4a}$$

This says that the smaller the particle separation, the farther the first minimum is from the chip center and that at $t = \lambda/2$ the first minimum is located at infinity (for any value of d). In practice, the farthest that the first minimum can be from the center is at $x = w$, the half width of the CCD chip, and for larger values of x (smaller separation between scattering points) the information contained in the modulation is
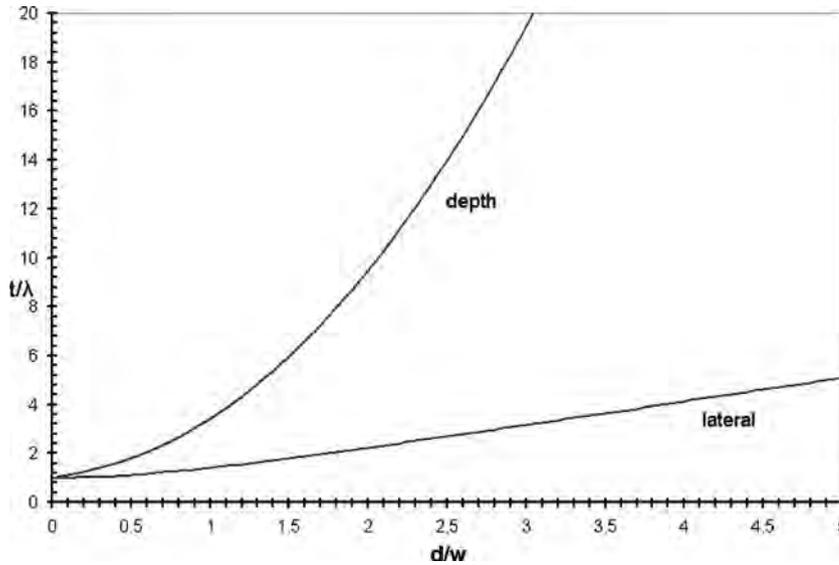
FIG. 9. Plot of the lateral and depth resolution functions with the condition that the first fringe modulation maximum be at the chip edge. Plotted is the separation t of scattering points divided by wavelength λ, as function of object-screen distance d, divided by w, the half width of the CCD chip.

not recorded and the two scatterers are not resolved. With an ideal screen (infinitely small pixels) of half width w, the smallest separation between scattering points allowed is then given by

$$t/\lambda = (1/2)\{1 + (d/w)^2\}^{1/2}. \qquad (4b)$$

We can also obtain expressions for the resolution in the direction normal to the screen.[15] If we apply the same criteria for fringe modulation as discussed above then the optimum perpendicular resolution δ is given by

$$\delta/\lambda = 1/\{1 - (d/w)/[1 + (d/w)^2]^{1/2}\}. \qquad (5)$$

Equations (4b) and (5) are plotted in Fig. 9 and the figure clearly shows the much lower resolution in the direction normal to the screen.

In practice, reconstructions of simulated holograms have shown that to resolve two scattering centers as two distinct objects requires that the first modulation maximum (not minimum) be captured on the CCD chip [for the first maximum the coefficient $\frac{1}{2}$ in Eq. (4a) and (4b) is replace by unity].[15] In addition we found that only fringes spaced more than 3 camera pixels apart contribute significantly to object reconstruction. In Fig. 8(b) the first modulation maximum is close to 3.3 mm from the chip center and the fringe spacing at that position is 50 μm or 8 pixels of 6 μm size. The hologram in Fig. 8(b) would thus satisfy the above criteria and would result in reconstructed images with about 1.6 μm resolution. At 5 μm separation of the scattering points, several modulation periods are visible with well spaced fringes, as shown in Fig. 8(c).

FRINGE SPACING AND PIXEL SIZE

If the fringe spacing near the first maximum is smaller than 3 pixels, then such fringes cannot be resolved by the CCD camera and they will not contribute significantly to image reconstruction and hence to improved resolution. The resolution criterion [Eq. (4a) and (4b)] does not take the relative size of pixel and fringe spacing into consideration. The fringe spacing depends on D and we can therefore expect a dependence of the resolution on D. When the fringe

spacing s is small compared to x, the distance of the fringe from the chip center, i.e., $s/x < 1$, then to a good approximation, the fringe spacing is given by

$$s = \lambda\{AB/(A - B)\}, \qquad (6)$$

where $A = [1 + (D/x)^2]^{1/2}$ and $B = [1 + (d/x)^2]^{1/2}$. This shows that the fringe spacing increases as expected when, for given object-screen distance, the source moves closer to the object.

As pointed out above, the fringe spacing should be larger than the pixel size. It is easy to calculate the fringe spacing from Eq. (6) and compare it with the size of a camera pixel. Figure 10 shows such a calculation for our submersible microscope geometry and for an effective wavelength of 422 nm. The concept of an effective wavelength is discussed in the following section. In Fig. 10 we plotted the fringe spacing in number of pixels as function of distance from the chip center. As seen from Fig. 10, the fringe spacing starts large near the chip center and rapidly narrows as one traverses the chip. The narrowing for the camera window side is much stronger than that for the source window as expected. The resolution criterion discussed above, where at least 3 pixels are needed to define a fringe, is indicated by the horizontal dash-dot line in Fig. 10. As shown, all fringes produced by a scattering point near the source window are separated by more than 3 pixels while scattering points near the camera window yield useful fringes only up to a distance of 0.55 mm from the chip center. If we use the condition that fringes with the 3 pixel cutoff separation must be located at the position of the first modulation maximum, then we can easily calculate the total number of fringes that will contribute to a hologram and hence to the reconstructed image. This total number of fringes between the chip center and the cutoff position on the chip is also shown in Fig. 10. For scattering points near the source window over 50 useful fringes (and a resolution of 1.5 μm) are obtained while the number of useful fringes near the camera window is no more than about 18 giving a resolution of 6.7 μm.
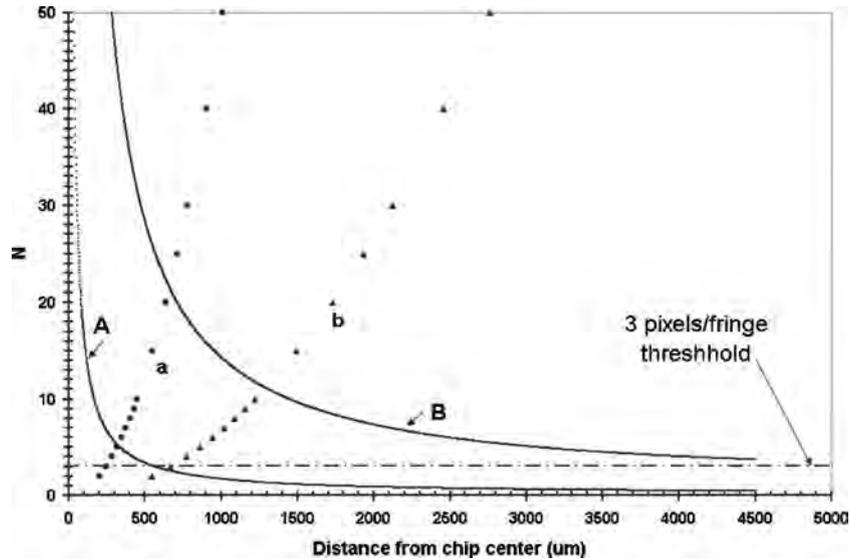
FIG. 10. Fringe spacing in number of pixels and total number of fringes as function of distance from the chip center for $\lambda = 422$ nm and a source-screen distance of 13.7 mm. CCD chip has a width of 6.6 mm and 6.4 μm square pixels. Curve (A) is the fringe spacing in number of camera pixels for a source-object distance of 5 mm (objects near the camera window) and points (a) are the corresponding calculated number of fringes between the chip center and a given point on the chip. The dot-dash line indicates the smallest fringe spacing that contributes to image reconstruction. Curves (A) and (a) suggest that near the camera window about 18 fringes contribute to image reconstruction. Curve (B) and points (b) are corresponding curves and points for a source-object distance of 1 mm (objects near the source window). Curve (B) and points (b) suggest that more than 50 fringes should contribute to image reconstruction resulting in high resolution for objects near the source window.

EFFECTIVE WAVELENGTH

In the submersible DIHM, the optic path from pinhole to CCD is not through a single medium but the path contains sections through water, glass, and air. In that case each section of length S_i produces its own phase shifts that depend on the refractive index of each section. The fringe pattern in that case can be described by an effective wavelength[16] given by

$$\lambda_{\text{eff}} = \lambda_1(s_1 + s_2 + \cdots + s_k)/(n_1 s_1 + n_2 s_2 + \cdots + n_k s_k).$$
(7)

Here λ_1 is the wavelength in air with refractive index $n_1 \cong 1$. A typical optical path for our microscope was $s_1 = 5.5$ mm in air, 4 mm in glass ($n_2 = 1.52$), and ~4 mm in water ($n_3 = 1.33$). The effective wavelength for green laser light ($\lambda_1 = 532$ nm) is then 422 nm and thus 21% shorter than in an all air medium. In practice, the sections with their different refractive indices result in a scaling of the diffraction pattern and the effective wavelength parameter makes allowance for this scaling. If the object is situated in a thin, low index slab, but the rest of the space between this slab and the CCD chip is occupied by a higher index medium such as water, then the hologram fringes will be determined largely by the short-wavelength in the high index medium. The long-wavelength illumination of the sample is thus transformed by the high index medium into a short-wavelength radiation that determines the phase shifts and structure of the hologram and hence the resolution of the microscope. The above analysis of DIHM resolution assumes ideal conditions such as an ideal point source of light and it neglects any additional reduction in resolution due to camera or other noise sources. The above analysis has been tested and repeatedly confirmed by reconstructions of simulated holograms and by many ex-

periments with aqueous suspensions of latex beads ranging in size from 0.5 to 10 μm.[15,16]

In addition to a change in wavelength, a change in refractive index at a boundary also causes refraction of light. The effect of refraction at an air-water interface on a fringe pattern, for example, is illustrated schematically in Fig. 11. In an all air medium, a reference ray might interfere with light scattered from a sample (the three beads at the air-water interface in Fig. 11) and produce a fringe at position x' that would not be recorded. With the beads immersed in water, however, the same ray would produce a fringe at position x and would thus be captured by the CCD. The high refractive index medium reduces the effective wavelength and brings more fringes on to the CCD chip through refraction. A high refractive index medium in front of the CCD chip thus increases the numerical aperture of DIHM just like oil does for oil immersion microscope objectives.
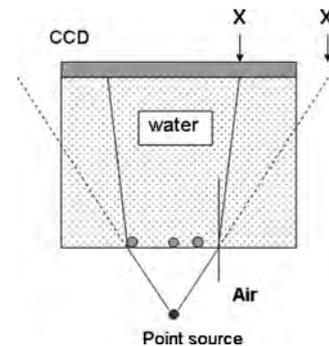

FIG. 11. Illustration of the effects of refraction at an air-water interface on the interference pattern. A ray that would fail to reach the CCD chip at position x' in an all air medium will fall on the chip in the presence of a high refractive index medium such as water. The overall effect of the high index medium is to compress the fringe pattern onto the CCD chip.
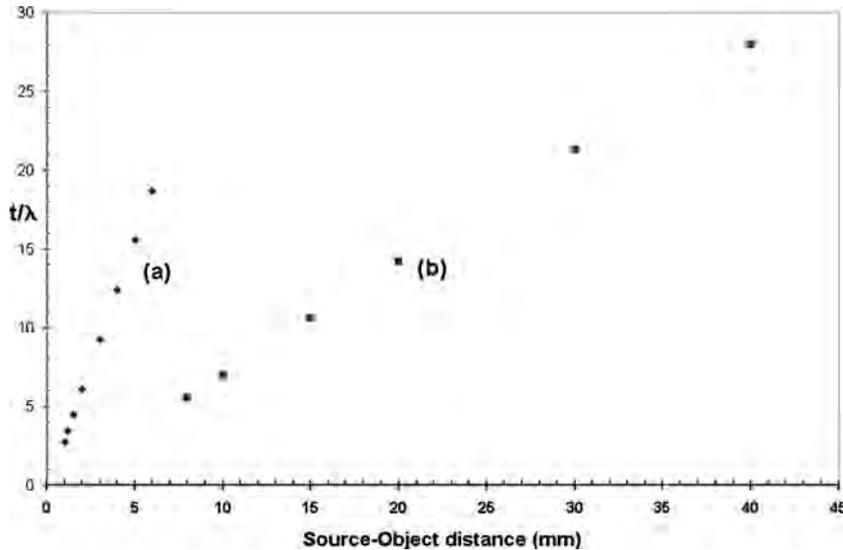
FIG. 12. Scattering point separation t divided by wavelength λ as function of source to object distance. (a) Calculation for a CCD chip area of 6.6 $\times$ 6.6 mm^2 with effective wavelength of 422 nm, source to screen distance D = 13.7 mm, and 6 μm size pixels. (b) Calculation for a chip area of 10 $\times$ 10 mm^2, effective wavelength of 402 nm, source to screen distance D = 60 mm, and 6 μm size pixels. The resolution criterion developed in the text suggests an optimum resolution of 1.5 μm for curve (a) and 6.8 μm for curve (b).

IMAGING VOLUME

The high depth of field of DIHM means that a single data set (a single hologram) can give high resolution throughout a larger sample volume than is possible with conventional optical microscopy. The resolution in DIHM is, however, a function of the source-sample distance and thus varies throughout the imaging volume. From the fringe spacing [Eq. (8)], with our two resolution criteria and with Eq. (4a) and (4b) we can calculate the resolution for a given source-sample distance. In Fig. 12. we show that the resolution is a nearly linear function of the source-sample distance. The cutoff in Fig. 12 at $t/\lambda \cong 3.5$ for the D = 13.7 mm data, and the corresponding limiting resolution of 1.5 μm, is caused by the 6.6 $\times$ 6.6 mm^2 chip reconstruction area employed for most of our SDIHM experiments. For larger reconstruction areas (hence larger chips), higher resolution would be obtainable. At the camera window, a 5 mm distance from the source, Fig. 12 gives t/λ = 16 and thus a resolution of 6.8 μm for an effective wavelength of 422 nm. From Fig. 12 we can thus estimate the volume of the imaging cone over which a given resolution range can be obtained. Figure 13(a) shows the imaging volume and field of view as function of distance from the source for a source-camera distance of 13.7 mm and a reconstruction area of 6.6 $\times$ 6.6 mm^2. The figure shows that 6.5 μm or better resolution is obtainable in a volume of 9 mm^3 and with a maximum field of view of 5 mm^2.

Larger CCD chips and hence larger reconstruction areas permit larger volumes to be sampled with still acceptable resolution for many marine applications. As an example, assume that in our present SDIHM the chambers are separated so that the source-camera distance is 60 mm. The effective wavelength for a green laser, in that case, would be 402 nm, and with a chip size of 10 $\times$ 10 mm^2 and 6 μm pixels (5.4 megapixel camera), Fig. 12 shows that the resolution range would be from 2.5 to $\sim$ 11 μm at 7 and 40 mm distances from the source, respectively. Hence the volume through which 11 μm or better resolution would be obtainable according to Fig. 13(b) is close to 1 cm^3. This is still small compared to the volumes sampled with comparable resolution by submersible holographic imaging systems that use high-resolution film for the recording of the holograms.[10,12] Our CCD based method, however, allows fast sampling of a single volume element or of a succession of different volume elements so that comparable information about particle distributions can be obtained. In fact, since successive holograms can be added or subtracted, a single data set could be created that contains information about particle distributions in a much larger volume than is represented in a single hologram. At the same time, microscopic organisms that swim closer to the source window will be imaged with much higher resolution than 11 μm and their identification will become possible.

SUMMARY

The simple design of our microscope coupled with the high image acquisition rate that is possible with digital cameras should make the instrument valuable for the studies and monitoring of plankton in coastal regions. The high resolution helps in the identification of marine organisms and the ability of DIH to capture the motion of organisms in their natural environment makes behavioral studies of plankton such as locomotion mechanisms, feeding habits, and interactions with surfaces (biofouling) possible. Unlike large volume imaging systems, our SDIHM gives micron size resolution with low power lasers, a simple CCD camera, and standard off-the-shelf SS chambers. As a result, our SDIHM is a low cost microscope that can be deployed from small motor boats or, in the future, from floating or bottom anchored platforms that relay holograms via satellite to laboratory computers. The maximum diameter of our microscope is given by the camera chamber flange with a diameter of 220 mm. This dimension can be reduced considerably and microscopes that, for example, fit into bore holes in arctic ice sheets could easily be constructed so that marine organisms below the arctic ice could be monitored on a continuing basis. So far the microscope records images when the vessel, from which it is operated, is stationary with respect to the water. Design ideas have already been developed that will allow the microscope to be towed, at selected depth, behind
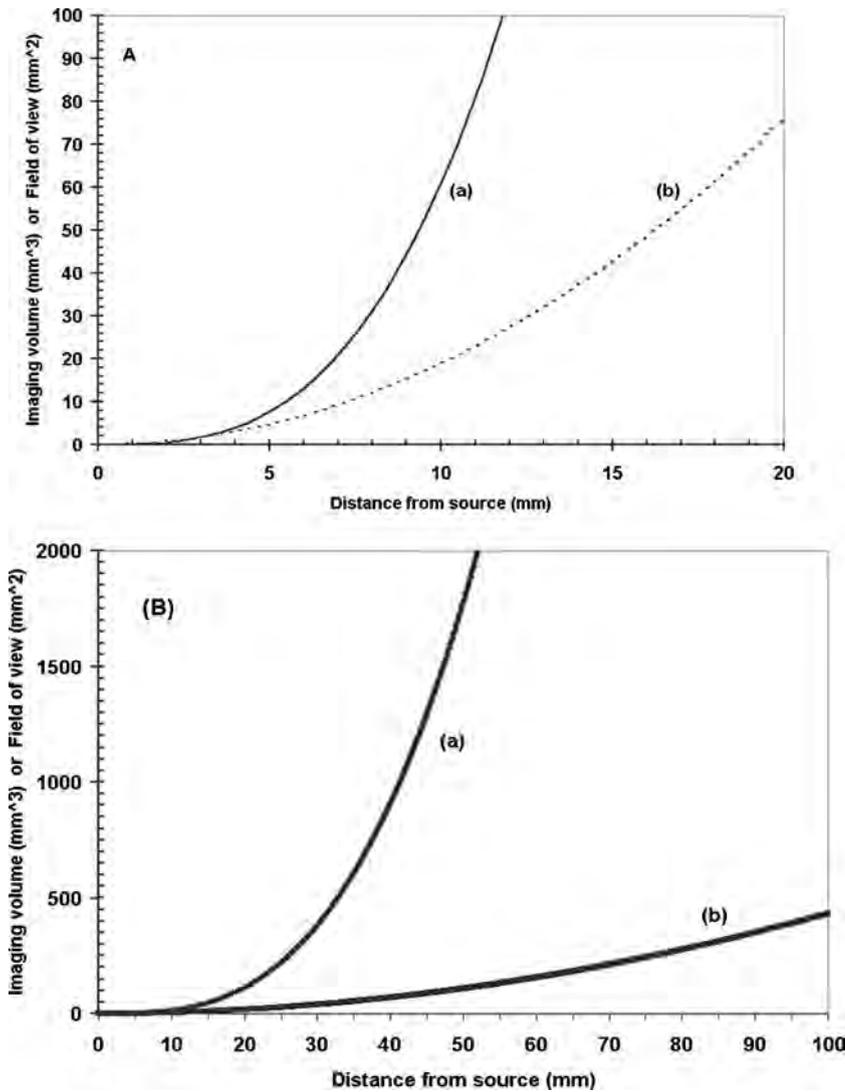
FIG. 13. (A) (a) Volume of the imaging cone between the point source and the base at given distance from the source. (b) Corresponding field of view as function of distance from the point source. (B) Enlarged region of (A) showing the volume and field of view for our SDIHM geometry. (a) Volume and (b) field of view.

a vessel so that better statistics for biomass determination in a given region can be obtained. At present, reconstruction of a single image plane from a 1024×1024 size hologram requires about 1 s. Holograms with a size of 512×512 can be reconstructed in $\frac{1}{4}$ of a second and still give useful resolution. Hologram reconstruction with hardware, such as digital signal processing (DSP) chips, for example, should shorten reconstruction times even further so that real time imaging with DIHM might become possible. An important feature of the SDIHM described here is its small size. This does not only mean that it can be deployed from small surface vessels, but also that it could form an important instrument package on submersible robotic research devices.

ACKNOWLEDGMENTS

[1] H. J. Kreuzer, Micron **26**, 503 (1995).

[2] H. J. Kreuzer, N. Pomerleau, K. Blagrave, and M. H. Jericho, Proc. SPIE **3744**, 65 (1999).

[3] W. Xu, M. H. Jericho, I. A. Meinertzhagen, and H. J. Kreuzer, Proc. Natl. Acad. Sci. U.S.A. **25**, 11301 (2001).

[4] H. J. Kreuzer, M. H. Jericho, I. A. Meinertzhagen, and W. Xu, J. Phys.: Condens. Matter **13**, 10729 (2001).

[5] W. Xu, M. H. Jericho, I. A. Meinertzhagen, and H. J. Kreuzer, Appl. Opt. **41**, 5367 (2002).

[6] W. Xu, M. H. Jericho, I. A. Meinertzhagen, and H. J. Kreuzer, Opt. Lett. **28**, 164 (2003).

[7] N. I. Lewis, A. D. Cembella, W. Xu, M. H. Jericho, and H. J. Kreuzer, Phycologia **45**, 61 (2006).

[8] L. O. Heflinger, G. L. Stewart, and C. R. Booth, Appl. Opt. **17**, 951 (1978).

[9] K. L. Carder, R. G. Stewart, and P. R. Betzer, J. Geophys. Res. **87**, 5681 (1982).

[10] E. Malkiel, O. Alquaddoomi, and J. Katz, Meas. Sci. Technol. **10**, 1142 (1999).

[11] E. Malkiel, J. N. Abras, and J. Katz, Meas. Sci. Technol. **15**, 601 (2004).

[12] J. Watson *et al.*, Meas. Sci. Technol. **12**, L9 (2001).

[13] R. B. Owen and A. A. Zozulya, Opt. Eng. (Bellingham) **39**, 2187 (2000).

[14] H. J. Kreuzer and R. A. Pawlitzek, LEEPS, Version 1.2, a software package for the simulation and reconstruction of low energy electron point source images and other holograms, 1993–1998.

[15] J. Garcia-Sucerquia, W. Xu, S. K. Jericho, P. Klages, M. H. Jericho, and H. J. Kreuzer, Appl. Opt. **45**, 836 (2006).

[16] J. Garcia-Sucerquia, W. Xu, M. H. Jericho, and H. J. Kreuzer, Opt. Lett. "Immersion Digital In-Line Holographic Microscopy," (in press, May 2006).